Supplemental Information

Supplemental Materials and Methods

Target gene sequencing of fractionated human CMML cells

Approximately 10 million viable bone marrow mononuclear cells (MCs) were sorted by FACS for the following populations: (1) Long-term hematopoietic stem cells (LT-HSCs) defined as Lin^- $CD34^+$ $CD38^-$ $CD123^-$ $CD45R\alpha^-$ $IL1RAP^-$ $CD99^-$ $CD25^-$ $CD90^+$; (2) Short-term hematopoietic stem cells (ST-HSCs) defined as Lin^- $CD34^+$ $CD38^-$ $CD123^-$ $CD45R\alpha^-$ $IL1RAP^-$ $CD99^-$ $CD25^-$ $CD90^-$; (3) Alternative 2 hematopoietic stem cells (A2HSCs) defined as Lin^- $CD34^+$ $CD38^-$ $CD123^-$ $CD45R\alpha^-$ $IL1RAP^-$ $CD99^-$ $CD25^+$; (4) Alternative 3 hematopoietic stem cells (A3HSCs) defined as Lin^- $CD34^+$ $CD38^-$ $CD123^-$ $CD45R\alpha^-$ $IL1RAP^-$ $CD99^+$; (5) common myeloid progenitors (CMP) defined as Lin^- $CD34^+$ $CD38^+$ $CD123^+$ $CD45R\alpha^-$; (6) granulocyte-macrophage progenitors (GMP) defined as Lin^- $CD34^+$ $CD38^+$ $CD123^+$ $CD45R\alpha^+$; (7) T-cells defined as $CD3^+$; (8) myeloid compartment defined as $CD33^+$; and (9) $CD45^+$ cells as positive controls. Bone marrow derived mesenchymal stem cells were generated and passaged twice to ensure no hematopoietic contamination as previously described [1]. Cells retrieved were whole genome amplified (WGA) as previously described if less than $1x10^5$ cells were retrieved post sort [2]. WGA or native DNA isolated from these populations were then subjected to a 49 gene next generation sequencing myeloid panel and sequenced on an Illumina instrument. Library preparation and variant calls were generated as previously described [2]. Genes tested include: ASXL1, BCOR, BCOR1, BRAF, CALR, CBL, CBLB, CEBPA, CSF3R, DNMT3A, ETV6, EZH2, FLT3, GATA1, GATA2, GNAS, HRAS, IDH1, IDH2, JAK1, JAK2, JAK3, KDM6A, KIT,

KMT2A/ MLL-PTD, KRAS, MEK1, MPL, MYD88, NOTCH1, NPM1, NRAS, PHF6, PML, PTEN, PTPN11, RAD21, RUNX1, SETBP1, SF3B1, SMC1A, SMC3, SRSF2, STAG2, TET2, TP53, U2AF1, WT1, ZRSR2. The target depth of sequencing was 1000x and variants were prioritized as previously described [2]. These studies were approved by the Moffitt Cancer Center Scientific Review Committee (SRC) and IRB.

Whole exome sequencing of sorted myeloid cells and T cells from CMML patient samples

$CD14^+$ monocytes and $CD3^+$ T cells were purified from CMML patient samples using magnetic beads (Mayo-1: StemCell Technologies; remaining samples: Miltenyi Biotec Inc.) and subjected for exome capture and NGS as described in [3,4]. Data were aligned to the hg19 reference genome.

CMML patient cohorts for survival analysis

This study was carried out at the Mayo Clinic in Rochester, Minnesota, after due approval from the Mayo Clinic Institutional Review Board (IRB-15-003786), and at Gustave Roussy Cancer Center in Villejuif, France, following the approval of the ethical committee Ile-de-France 1 (DC-2014-2091). Several patient cohorts were analyzed. In all cases, diagnosis was according to 2016 iteration of the WHO classification of myeloid malignancies [5]. Cohort # 1 included 48 CMML patients whose paired MC samples were collected in chronic phase and in leukemia transformation to perform WES. Cohort # 2 of 18 CMML patients was used to perform WES on samples serially collected along disease progression. This cohort had been described previously [3]. Cohort # 3 was made of 350 CMML patients

collected at Mayo Clinic; genetic abnormalities were screened using a 36-gene panel targeted NGS assay. Cohort # 4 was made of CMML patient samples collected in France (n=417) and in Austria (n=322) with molecular information obtained by NGS using a 38-gene panel targeted NGS assay. Peripheral blood (PB) and bone marrow (BM) samples were collected in EDTA tubes after due informed consent. MCs were collected on Ficoll-Hypaque whereas $CD14^-$ and $CD3^+$ cells were isolated using magnetic beads via the AutoMACS system (Miltenyi Biotech). In 5 cases, buccal mucosa cells were used as germline control cells.

Complete blood count (CBC) and histopathology.

CBC analysis was performed using a Hemavet 950FS (Drew Scientific). Mouse tissues were fixed in 10% neutral buffered formalin (Sigma-Aldrich) and further processed at the Experimental Pathology Laboratory of the University of Wisconsin Carbone Cancer Center.

Flow cytometric analysis of hematopoietic tissues

For lineage analysis of PB, BM, and spleen (SP), flow cytometric analyses were performed as previously described [6]. Lin^- $Sca1^+$ $c\text{-}Kit^+$ (LSKs) and myeloid progenitors (MPs, defined as Lin^- $Sca1^-$ $c\text{-}Kit^+$) in BM and SP were analyzed as described in [7]. Hematopoietic stem cells (HSCs, defined as $CD41^-$ Lin^- $CD48^-$ $Sca1^+$ $c\text{-}Kit^+$ $CD150^+$) and multipotent progenitors (MPPs, defined as $CD41^-Lin^-$ $CD48^-$ $cKit^+$ $Sac1^+$ $CD150^-$) in BM and SP were analyzed as described by Kong et al. [8]. In $CD4^+$ and $CD8^+$ single-positive T cells, naïve T cells (defined as $CD62L^+$ $CD44^-$), effector T cells (defined as $CD44^+$ $CD62L^-$), central memory T cells (defined as $CD62L^+$ $CD44^+$), and exhausted T cells

(defined as PD-1^{+} TIGIT^{+} LAG3^{+}) were analyzed as previously described in [9,10]. The stained cells were analyzed on a LSR II (BD Biosciences).

Antibodies specific for the following surface antigens were purchased from Thermo Fisher Scientific: CD45.2 (104), CD45.1 (A20), B220 (RA3-6B2), CD19 (eBio1D3), Thy1.2 (53-2.1), Mac-1 (M1/70), Gr-1 (RB6-8C5), CD4 (GK1.5), CD8 (53-6.7), CD3 (145-2C11), IgM (II/41), IL7Rα (A7R34), Sca-1 (D7), TER119 (TER-119), CD34 (RAM34), cKit (2B8), FcγRII/III (93). Antibodies specific for the following surface antigens were purchased from BioLegend: CD150 (TC15-12F12.2), PD-1 (29F), CTLA4 (UC10-4B9), TIGIT (LG9), LAG3 (C9B7W), PD-L1 (10F), PD-L2 (TY25), CD86 (GL1), CD80 (16-10A1), CD155 (4.24.1), CD44 (IM7), and CD62L (MEL-14).

Cell cycle analysis

Cell cycle analysis was performed essentially as previously described [8]. Briefly, bone marrow cells were labeled with following antibodies for myeloid progenitor cells: biotin-conjugated antibodies against B220 (RA3-6B2), CD3 (145-2C11), CD4 (GK1.5), CD8 (53-6.7), Gr-1 (RB6-8C5), CD127 (A7R34), CD19 (eBio1D3), IgM (II/41) and TER-119 (TER-119) followed by PE-Cy7 Streptavidin, PerCP Cy5.5-Sca1 (D7), APC-eFluro 780-c-Kit (2B8). Stained cells were fixed in 2% Paraformaldehyde (Electron Microscopy Sciences)/PBS, and permeablized in 0.1% Saponin (Sigma)/PBS containing PE-Ki67 (BD Biosciences) and DAPI (Thermo Fisher Scientific). All of the antibodies were purchased from Thermo Fisher Scientific unless specified. The stained cells were analyzed on a LSRII (BD Biosciences).

Colony assay

$5x10^4$ bone marrow cells were plated in duplicate in semisolid medium MethoCult M3234 (Stem Cell Technologies) supplemented without or with mGM-CSF or mIL-3 (PeproTech) according to the manufacture's protocol. The colonies were counted after 7 days in culture.

Flow cytometric analysis of phospho-ERK1/2

Bone marrow cells were deprived of serum and cytokines, and then stimulated with or without GM-CSF as previously described [11]. Surface proteins were detected with PE-conjugated antibodies (Thermo Fisher Scientific unless specified) against B220 (RA3-6B2), Gr-1 (RB6-8C5), CD3 (17A2, Biolegend), CD4 (GK1.5), CD8 (53-6.7), TER119 (TER-119), and APC-eFluro780-conjugated anti-CD117/c-Kit (2B8) antibody. p-ERK1/2 (phosphorylated ERK1/2) was detected by a primary antibody against p-ERK (Thr202/Tyr204; Cell Signaling Technology) followed by APC conjugated donkey anti-rabbit F(ab')2 fragment (Jackson ImmunoResearch). The stained cells were analyzed on a LSRII (BD Biosciences).

Transplantation of primary *Nras$^{G12D/+}$; Asxl1$^{-/-}$* CMML and AML cells

CD45.1$^+$ recipient mice were sub-lethally irradiated (4.0 Gy) using an X-Rad 320 irradiator (Precision X-Ray) and transplanted with $1x10^6$ BM or $2x10^6$ SP/liver cells from

moribund *Nras*$^{G12D/+}$*; Asxl1*$^{-/-}$ mice with AML phenotype, or 1x10^6 BM cells from moribund *Nras*$^{G12D/+}$*; Asxl1*$^{-/-}$ mice with CMML phenotype.

WES of mouse leukemia cells and data analysis

Genomic DNAs were extracted from BM cells and tail tissues of moribund *Nras*$^{G12D/+}$*; Asxl1*$^{-/-}$ mice with CMML or AML using Gentra Puregene Cell Kit (Qiagen). Whole-exome targeted capture was carried out using the SureSelect XT Mouse Exome Kit, 49.6 Mb (Cat# 5190-4641; Agilent Technologies). The captured and amplified exome library was sequenced with 100bp paired-end reads on an Illumina HiSeq4000. Analysis was performed by Mayo Bioinformatics Core. Briefly, all samples were aligned to mouse genome-built version mm10 using bwa-mem version 0.7.10. Realignment and recalibration steps implemented in the GATK version 3.6 were subsequently applied. All variant calls were made through Mutect v1.1.7 [12] and Strelka v2.8.4 [13]. Each variant was annotated using Annovar [14]. Further filtering was applied to identify high confidence somatic mutations. Mutations meeting any of the following criteria were removed: 1) Variants in non-coding regions; 2) Number of reads supporting alternative allele < 5 or total depth < 10 reads; 3) Fail quality filter was applied.

RNA-Seq analysis of mouse BM Lin$^-$ cKit$^+$ cells

Total RNAs were isolated from 50,000 sorted Lin$^-$ c-Kit$^+$ cells of moribund *Nras*$^{G12D/+}$*; Asxl1*$^{-/-}$ (CMML, n=3 and AML, n=3) mice and age-matched control (n=3), *Asxl1*$^{-/-}$ (n=3), and *Nras*$^{G12D/+}$ (n=3) mice using RNeasy Micro Kit (Qiagen). RNA-Seq libraries

were prepared using SMARTer® Stranded Total RNA-Seq Kit v2 - Pico Input Mammalian (Clontech). RNA-Seq was performed using an Illumina HiSeq 4000 system at the NUSeq Core facility, Northwestern University. Sequencing data (>40 millions reads per sample) were analyzed by BioInfoRx, Inc. Raw sequencing data quality was evaluated using FastQC, and reads were mapped to the mouse genome mm10 using Subread package. Gene level expression values were obtained using FeatureCount from Subread package. Data normalization and differential expression analysis were performed using limma package in R. Raw sequencing data will be deposited to SRA database upon manuscript acceptance. Gene set enrichment analysis (GSEA) was performed as previously described [15] using hallmark gene sets in the GSEA databases. Gene Ontology (GO) analysis was analyzed using the gene ontology resource as previously described [16].

RNA-Seq analysis of human CMML patient samples

Library preparation for the RNA samples was done using Illumina TruSeq Stranded Total RNA and sequencing was done using Illumina HiSeq 4000, 100 cycles x 2 paired-end reads at Mayo Clinic, Rochester, MN. RNA-seq sequencing reads were processed through the MAPRSeq v2.0. bionformatics workflow as described in [17]. Libraries were sequenced on an Illumina HiSeq2500 platform to a read depth of approximately 50 million reads per sample. Reads were aligned to the human genome (GRCh38/hg38) using the HISAT2 aligner [18]. Read counts were generated using featureCounts with reference to Homo_sapiens.GRCh38.90.gtf annotation file from Ensembl [19,20].

ENCODE ChIP-seq data analysis

ChIP-seq data of various histone marks at the *PD-L1*and *CD86* loci were generated in K562 AML cell line using ENCODE database deposited by the Broad Institute and the Bernstein lab (Massachusetts General Hospital/Harvard Medical School). ChIP-seq data of AP-1 complex transcript factors at the *PD-L1*and *CD86* loci were generated in K562 AML cell line using ENCODE database deposited by Michael Snyder (Stanford University), Mark Gerstein and Sherman Weissman (Yale University), Peggy Farnham (University of Southern California), and Kevin Struhl (Harvard Medical School). ChIP-seq data of Jun and Jund at the *PD-L1*and *CD86* loci were generated in mouse CH12 cell line using ENCODE database deposited by Michael Snyder (Stanford University).

Chromatin immunoprecipitation-qPCR (ChIP-qPCR)

$2x10^7$ BM cells from moribund NA-AML mice and age-matched control, *Asxl1*$^{-/-}$, and *Nras*$^{G12D/+}$ mice were directly cross-linked with 1% formaldehyde for 15 min, and quenched with 125mM glycine for 5 min. Cells were washed twice with ice-cold PBS and then lysed with 10ml Buffer I (10mM HEPES pH 7.0, 10mM EDTA, 0.5mM EGTA, 0.25% Triton X-100, and 0.5mM PMSF) with rotation for 10 min at 4 °C. The crude nuclei were pelleted by centrifugation (1500 rpm, 4 min). Crude nuclei were washed with 10ml Buffer II (10mM HEPES pH 7.0, 200mM NaCl, 1mM EDTA, 0.5mM EGTA and 0.5mM PMSF) while rotating for 10 min at 4 °C, and pelleted by centrifugation at 1500 rpm for 4 min. Nuclei were resuspended in 1ml nuclear lysis buffer (50mM Tris-HCl pH 8.1, 10mM EDTA, 1% SDS, 1mM PMSF, and 1x protease inhibitor cocktail (11836170001, Roche)), and incubated on ice for 10 min. Chromatin was sheared by

sonication in an ice-water bath at 4 °C using a Branson Sonifier 450 with a microtip (40% amplitude, 3 sec on, 10 sec off, 3 min of total pulse time). The supernatant was collected by centrifugation (15,000 rpm, 10 °C, 15 min). The H3K27Ac (Cat# 8173, Cell Signaling) antibody, c-Jun (Cat# ab32137, Abcam) antibody and normal rabbit IgG (Cat# sc-2027, Santa Cruz) were used for ChIP assays according to the previously described method [21]. Primers for H3K27Ac-ChIP-qPCR were designed based on the H3K27ac binding peaks in ENCODE database (ENCSR863VHE): PD-L1-F: 5' ACTTAACCGTAGCCTCAAGCC 3'; PD-L1-R: 5' TCCTAAGTGTTGTAGGGTCGC 3'; CD86-F: 5' GTTTCCTGCGGAGATGGGTC 3'; CD86-R: 5' TAGGTCGAACTATGCGACGG 3'; Jund-F: 5' TAGCTGGCTCAGT CGTTTGG 3'; Jund-R: 5' AGTTGTTGCCTCAGAGAGCC 3'; Jun-F: 5' ACAGAGC GATGCGGGTTAAA 3'; Jun-R: 5' GGTTCCGAACACCGCAAATC 3'; Fos-F: 5' GTCACCTAACCCTTCCCAGC 3'; Fos-R: 5' CCTACGTGTCACCGTGGAAA 3'. Primers for Jun-ChIP-qPCR were designed based on the c-Jun binding peaks in ENCODE database (ENCSR000ERO): PD-L1-F:5'GAAACAGGTGGAGGAG TGGG 3'; PD-L1-R: 5' CTCCACAGAGAAGGCAAGGG 3'; CD86-F: 5' GAAACC GAGGACCAGACACC 3'; CD86-R: 5' GGTAAGGAAAGCGGTTGGGA 3'. The qPCR assays (SYBR Green Supermix, #1708886, Bio-Rad) were performed following the manufacture's protocol.

Cell culture and drug treatment

Bone marrow cells from moribund *Nras*$^{G12D/+}$*; Asxl1*$^{-/-}$ mice with AML were cultured in SFEM (Stem Cell Technologies) with 10% FBS (Invitrogen), 0.2ng/ml mGM-CSF

(PeproTech). Cells were seeded at $2x10^5$/ml in triplicate in 96-well plates in the presence of DMSO, various concentrations of trametinib (ChemieTek) and/or GSK525762 (ChemieTek), or 4μM AP-1 inhibitor, SR11302 (CAS 160162-42-5, R&D Systems). After 5 days in culture, cell viability was determined using the CellTiter Glo Assay (Promega) according to the manufacturer's instructions. Surface expression of immune checkpoint ligands were analyzed in Lin^- c-Kit^+ cells using flow cytometry.

Lentivirus packaging and transduction

$3x10^6$ HEK293T cells were cultured in a 10-cm dish overnight before transfecting with 10 μg of plasmid (2μg VSVG, 4μg PAX2, and 4μg GIPZ lentiviral control shRNA (RHS4346, Horizon Discovery) or Jun shRNA (RMM4532-EG16476, Horizon Discovery) using polyethylenimine (#23966, Polysciences). Supernatant containing the virus was harvested 48 hours after infection and concentrated ~100-fold using Lenti-X Concentrator (#631231, Takara). 1 x 10^5 NA-AML cells were seeded into 24-well plate and infected with 100μl concentrated lentivirus soup containing 5 μg/ml of polybrene by centrifugation at 1,000 x g for 90 min at RT. Surface expression of PD-L1 and CD86 were analyzed in Lin^- c-Kit^+ GFP^+ cells 72 hours after infection using flow cytometry.

Western blot analysis

Primary antibodies against H3K27m3 (Cat# 9733), H3K4m3 (Cat# 9751), H3K4m1 (Cat# 5326), H3K27ac (Cat# 8173) and H3 (Cat# 4499) were purchased from Cell Signaling Technology. Antibody against β-actin (Cat# sc-1616-R) was purchased from Santa Cruz Biotechnology. HRP-conjugated goat anti-mouse (Cat# 115-035-003) and HRP-

conjugated goat anti-rabbit (Cat# 111-035-003) secondary antibodies were purchased from Jackson ImmunoResearch. Chemiluminescent HRP substrate (Cat# WBKLS055) were purchased from Millipore. The chemiluminescent signals were detected using ImageQuant LAS4000 (GE Healthcare) and quantified using ImageStudioLite (LI-COR) software.

Secondary bone marrow transplantation and drug treatment

Sub-lethally irradiated (4.0 Gy using an X-Rad 320 irradiator, Precision X-Ray) CD45.1^{+} mice were transplanted with 0.5x10^{6} BM cells from moribund *Nras*$^{G12D/+}$*; Asxl1*$^{-/-}$ primary recipients with AML phenotype. For treatment with JAK and MEK inhibitors, secondary recipients were randomly separated into two groups at 2 weeks after transplantation and treated with vehicle or combined ruxolitinib (30mg/kg, ChemieTek) and trametinib (0.5mg/kg), via oral gavage daily until the moribund stage. For treatment with BET and MEK inhibitors, secondary recipients were randomly separated into two or four groups at 2 weeks after transplantation and treated with vehicle, GSK525762 (15mg/kg), trametinib (0.5mg/kg), or combined GSK525762 (15mg/kg) and trametinib (0.5mg/kg), via oral gavage daily until the moribund stage. In combined GSK525762 and trametinib treatment, the compounds were administered ~8 hours apart to avoid potential toxicities. Ruxolitinib was resuspended in water supplemented with 0.5% dimethylacetamide (Sigma) and 0.5% methocellulose (Sigma). Trametinib was resuspended in water supplemented with 1% methycellulose and 0.2% SDS (Sigma). GAK525762 was resuspended in water supplemented with 0.5% hydroxypropyl methycellulose (Sigma) and 0.2% tween 80 (Sigma).

T cell cytotoxicity assay

Sub-lethally irradiated (4.0 Gy using an X-Rad 320 irradiator, Precision X-Ray) CD45.1$^+$ mice were transplanted with 0.25x10^6 BM cells from moribund NA-AML mice. Recipients were randomly separated into two groups 2 weeks after transplantation and treated with vehicle or combined GSK525762 (15mg/kg) and trametinib (0.5mg/kg) via oral gavage daily until the vehicle treated group reached the moribund stage. Leukemia cells (CD45.2$^+$) were sorted from splenocytes of vehicle treated mice. Host derived CD45.1$^+$ CD8$^+$ T cells were sorted from splenocytes of vehicle and combo treated mice. 2x10^4 leukemia cells were co-cultured with CD8$^+$ T cells in 48-well plates at the indicated target: effector ratios. After 48 hours of co-culture, total live cell numbers were counted and CD45.2$^+$% was determined using flow cytometry. Live leukemia cell numbers were calculated using total live cell numbers multiplied by CD45.2$^+$% in total live cells.

qRT-PCR analysis of *Fos, Fosb, Jun, Junb, Jund, Atf3, Flt3, PD-L1 and CD86* expression

Lin$^-$ c-Kit$^+$ cells from moribund *Nras$^{G12D/+}$; Asxl1$^{-/-}$* mice with AML and age-matched control, *Asxl1$^{-/-}$*, and *Nras$^{G12D/+}$* mice, sh-Control or sh-Jun lentivirus transfected (GFP$^+$) c-Kit$^+$ cells and CD45.2$^+$ leukemia cells from secondary recipients with *Nras$^{G12D/+}$; Asxl1$^{-/-}$* AML cells were flow sorted into RNAprotect Cell Reagent (Qiagen). Total RNAs were extracted using RNeasy Micro Kit (Qiagen). cDNAs were synthesized using iScript™ Reverse Transcription Kit (Bio-Rad). Real-time PCR reactions were performed on a

CFX96 Real-Time System (Bio-Rad) using the primers specific for *Fos* (F: 5'-GCAGATCTGTCCGTCTCTAG-3', R: 5'-GGTGGGG AGTCCGTAAGGAT-3'), *Fosb* (F: 5'-GCACAACCACCAGTGGACCT-3', R: 5'-TGTTCCGCTCTCTGCGAACC-3'), *Jun* (F: 5'-CTATCGACATGGAGTCTCAG-3', R: 5'-TAGCCGAGCGATCCGCTCCA-3'), *Junb* (F: 5'-GTCTACACCAACCTCAGCAG-3', R: 5'-TGGTGCATGTGGGAGGTAGC-3'), *Jund* (F: 5'-GCGCAAGCTGGAGCGT ATCT-3', R: 5'- TGGCAGCCGCTGTTGACGTG-3'), *Atf3* (F: 5'-GCTTCAACATCCA GGCCAGG-3', R: 5'-GGATGGCGAATCTCAGCTCTTCC-3'), *Flt3* (F: 5'-GAACCC TTACCCTGGCATTC-3', R: 5'-GCTTCCTTGAGTCAAAAGCC-3'), *PD-L1*(F: 5'-TGTCTCCATGGCAGAAGCAG-3', R: 5'-AGGAGAGGCAGTAGCTGTCA-3'), CD86 (F: 5'-TCACAACTTAGCAGGCAGCA-3', R: 5'- CCTGGTTTTGAGTGCTTG GC-3') (Integrated DNA Technologies, Inc). The cycling condition is: 95 °C 3 min, (95 °C 15 sec, 60 °C 1 min) x 40 cycles). *β-actin* was chosen as the house keeping gene as previously described [22].

Flow analysis of histone marks

Expression levels of histone marks were quantified in CD45.2$^+$ BM leukemia cells from vehicle or combo drug treated mice using flow cytometry following the manufacture's protocol. The following antibodies were purchased from Cell Signaling Technology: PE-H3K4me1 (D1A9), PE-H3K4me3 (C42D8), Alexa 488-H3K27ac (D5E4), and Alexa 647-H3K27me3 (C36B11).

CMML patient-derived xenograft (PDX) model and drug treatment

The NOD.Cg-*Prkdc*^{scid} *Il2rg*^{tm1Wjl}/SzJ-SGM3 (NSGS) mice were used for the PDX experiments [23]. 1.78 million BM nucleated cells from *RAS* and *ASXL1* double mutant CMML patient were transplanted into irradiated NSGS (250 cGy, a cesium source irradiator) mice through tail vein injection 24 hours after irradiation. At 5 days after transplantation, mice were randomly separated into two groups and treated with vehicle or combined trametinib and GSK525762 as described above every day from Monday to Friday until the moribund stage.

Statistics.

Kaplan-Meier survival analysis was performed and survival differences between groups were assessed with the Log-rank test, assuming significance at $P < 0.05$. Unpaired 2-tailed Student's tests were used to determine the significance between two data sets, assuming significance at $P < 0.05$.

Supplemental References

1. Mailloux AW, Zhang L, Moscinski L, et al. Fibrosis and subsequent cytopenias are associated with basic fibroblast growth factor-deficient pluripotent mesenchymal stromal cells in large granular lymphocyte leukemia. *J Immunol*. 2013;191(7):3578-3593.
2. Zhang Q, Ball MC, Zhao Y, et al. Intrapatient functional clonality deconvoluted by coupling intracellular flow cytometry and next-generation sequencing in human leukemia. *Leukemia*. 2018;32(2):532-538.
3. Merlevede J, Droin N, Qin T, et al. Mutation allele burden remains unchanged in chronic myelomonocytic leukaemia responding to hypomethylating agents. *Nat Commun*. 2016;7:10767.
4. Carr RM, Vorobyev D, Lasho T, et al. RAS mutations drive proliferative chronic myelomonocytic leukemia via a KMT2A-PLK1 axis. *Nat Commun*. 2021;12(1):2901.
5. Arber DA, Orazi A, Hasserjian R, et al. The 2016 revision to the World Health Organization classification of myeloid neoplasms and acute leukemia. *Blood*. 2016;127(20):2391-2405.

6. Zhang J, Wang J, Liu Y, et al. Oncogenic Kras-induced leukemogeneis: hematopoietic stem cells as the initial target and lineage-specific progenitors as the potential targets for final leukemic transformation. *Blood*. 2009;113(6):1304-1314.
7. Wang JY, Liu YG, Li ZY, et al. Endogenous oncogenic Nras mutation initiates hematopoietic malignancies in a dose- and cell type-dependent manner. *Blood*. 2011;118(2):368-379.
8. Kong G, Wunderlich M, Yang D, et al. Combined MEK and JAK inhibition abrogates murine myeloproliferative neoplasm. *J Clin Invest*. 2014;124(6):2762-2773.
9. Sckisel GD, Mirsoian A, Minnar CM, et al. Differential phenotypes of memory CD4 and CD8 T cells in the spleen and peripheral tissues following immunostimulatory therapy. *J Immunother Cancer*. 2017;5:33.
10. Kurtulus S, Sakuishi K, Ngiow SF, et al. TIGIT predominantly regulates the immune response via regulatory T cells. *J Clin Invest*. 2015;125(11):4053-4062.
11. Wang JY, Liu YG, Li ZY, et al. Endogenous oncogenic Nras mutation promotes aberrant GM-CSF signaling in granulocytic/monocytic precursors in a murine model of chronic myelomonocytic leukemia. *Blood*. 2010;116(26):5991-6002.
12. Cibulskis K, Lawrence MS, Carter SL, et al. Sensitive detection of somatic point mutations in impure and heterogeneous cancer samples. *Nat Biotechnol*. 2013;31(3):213-219.
13. Saunders CT, Wong WS, Swamy S, Becq J, Murray LJ, Cheetham RK. Strelka: accurate somatic small-variant calling from sequenced tumor-normal sample pairs. *Bioinformatics*. 2012;28(14):1811-1817.
14. Wang K, Li M, Hakonarson H. ANNOVAR: functional annotation of genetic variants from high-throughput sequencing data. *Nucleic Acids Res*. 2010;38(16):e164.
15. Subramanian A, Tamayo P, Mootha VK, et al. Gene set enrichment analysis: a knowledge-based approach for interpreting genome-wide expression profiles. *Proc Natl Acad Sci U S A*. 2005;102(43):15545-15550.
16. The Gene Ontology C. Expansion of the Gene Ontology knowledgebase and resources. *Nucleic Acids Res*. 2017;45(D1):D331-D338.
17. Kalari KR, Nair AA, Bhavsar JD, et al. MAP-RSeq: Mayo Analysis Pipeline for RNA sequencing. *BMC Bioinformatics*. 2014;15:224.
18. Kim D, Langmead B, Salzberg SL. HISAT: a fast spliced aligner with low memory requirements. *Nat Methods*. 2015;12(4):357-360.
19. Zerbino DR, Achuthan P, Akanni W, et al. Ensembl 2018. *Nucleic Acids Res*. 2018;46(D1):D754-D761.
20. Liao Y, Smyth GK, Shi W. featureCounts: an efficient general purpose program for assigning sequence reads to genomic features. *Bioinformatics*. 2014;30(7):923-930.
21. Zeng H, Xu W. Ctr9, a key subunit of PAFc, affects global estrogen signaling and drives ERalpha-positive breast tumorigenesis. *Genes Dev*. 2015;29(20):2153-2167.
22. Kong G, You X, Wen Z, et al. Downregulating Notch counteracts Kras(G12D)-induced ERK activation and oxidative phosphorylation in myeloproliferative neoplasm. *Leukemia*. 2018.
23. Yoshimi A, Balasis ME, Vedder A, et al. Robust patient-derived xenografts of MDS/MPN overlap syndromes capture the unique characteristics of CMML and JMML. *Blood*. 2017;130(4):397-407.

Supplemental Figure Legends

Figure S1. Oncogenic *NRAS* serves as a founding or progression mutation in CMML. (A) Target gene sequencing of hematopoietic stem and progenitors in CMML. Bone marrow mononuclear cells (BMNCs) from 3 representative CMML patients were sorted into four immunophenotypically defined hematopoietic stem cells (HSCs), common myeloid progenitors (CMPs), granulocyte-macrophage progenitors (GMPs), T-cells, and myeloid cells ($CD33^+$) as described in Methods. $CD45^+$ cells were additionally sequenced as a positive control. Bone marrow derived mesenchymal stem cells passaged twice (MSC2) were used as germline controls. Variant allele frequencies were labeled in each fraction, and squares with dashes represents samples in which insufficient DNA was recovered even after whole genome amplification. (B) Whole exome sequencing of additional CMML samples. Fish plots of representative CMML cases that may acquire a *NRAS* mutation at the time of CMML initiation (left) or during CMML progression (right).

Figure S2. Evaluation of 10-weeks old *Nras$^{G12D/+}$* mice.

Control (C; *Vav-Cre*) and *Nras$^{G12D/+}$; Asxl1$^{-/-}$* (NA) mice were sacrificed at 6 weeks old, while *Nras$^{G12D/+}$* (Nras) mice were sacrificed at 10 weeks old. (A) Quantification of spleen weight. (B) Quantification of white blood cells (WBC) in peripheral blood. (C) Quantification of numbers of monocytes and neutrophils in peripheral blood. Data are presented as mean + SD. ns, not significant. * $P<0.05$.

Figure S3. Multiple recurrent mutations are identified in *Nras$^{G12D/+}$; Asxl1$^{-/-}$* CMML samples.

Four paired tail DNA (non-leukemia control) and bone marrow DNA from moribund *Nras$^{G12D/+}$; Asxl1$^{-/-}$* CMML mice were subjected for whole exome sequencing as described in Methods. (A) Recurrent mutations (mutated in >= 3/4 mice) and their variant allele frequencies are shown. The frequencies of mutated human orthologs are determined from a cohort of 174 CMML patient samples. Recurrent mutations identified in both NA-CMML and NA-AML are highlighted in yellow. (B) Gene Ontology analysis of recurrently mutated genes (mutated in >= 2/4 mice). The representative molecular functions are shown with numbers of genes in each category and corresponding False Discovery Rate.

Figure S4. Multiple recurrent mutations are identified in *Nras$^{G12D/+}$; Asxl1$^{-/-}$* AML samples.

Six paired tail DNA (non-leukemia control) and bone marrow DNA from moribund *Nras$^{G12D/+}$; Asxl1$^{-/-}$* AML mice were subjected for whole exome sequencing as described in Methods. (A) Recurrent mutations (mutated in >= 4/6 mice) and their variant allele frequencies were shown. The frequencies of mutated human orthologs are determined from AML patient databases and a cohort of 36 paired CMML and AML patient samples (Mayo Clinic). Recurrent mutations identified in both NA-CMML and NA-AML are highlighted in yellow. (B) Gene Ontology analysis of recurrently mutated genes (mutated in >= 3/6 mice). The representative molecular functions are shown with numbers of genes in each category and corresponding False Discovery Rate. (C) Venn diagram illustrating the mutated genes identified in both *Nras$^{G12D/+}$; Asxl1$^{-/-}$* (NA)-CMML and NA-AML samples.

Figure S5. RNA-seq analysis of CMML patient cells reveals aberrant regulation of immune system.

(A) Heatmap shows differentially expressed genes (DEGs) in *NRAS/ASXL1* double mutant CMML patient samples vs samples from healthy donors (fold change ≥2 and False Discovery Rate (FDR) <0.05). (B) Gene Ontology analysis of DEGs. The representative biological processes are shown with numbers of genes in each category and corresponding FDR. (C) ConsensusPathDB analysis (http://cpdb.molgen.mpg.de/) of DEGs. The size of the circle reflects the number of genes in each set. The color of circle means p value. All the pathways shown here are significantly enriched ($P < 0.05$).

Figure S6. Upregulation of Flt3 surface expression in *Nras$^{G12D/+}$; Asxl1$^{-/-}$* AML cells

Representative histograms showing surface expression levels of Flt3 in bone marrow Lin$^-$ c-Kit$^+$ cells (left; the dash line defines Flt3$^+$ cells) and Lin$^-$ c-Kit$^+$ Flt3$^+$ cells (right) from moribund *Nras$^{G12D/+}$; Asxl1$^{-/-}$* AML mice. MFI, median fluorescence intensity.

Figure S7. NA-CMML and NA-AML cells show similar sensitivity to Flt3 inhibitor treatment as control BM cells.

Control, NA-CMML, and NA-AML cells were cultured in triplicate in 96-well plates in the presence of DMSO or various concentrations of Type I and Type II Flt3 inhibitors for 7 days. Cell numbers were quantified using the CellTiter-Glo assay (Promega). Data are presented as mean + SD.

Figure S8. Identification of AP-1 TF binding peaks at the potential enhancer regions at the *PD-L1* and *CD86* loci.

(A) H3K4me1, H3K4me3, H3K9ac, H3K9me3, H3K27ac, H3K27me3, FOS, JUN and JUND binding peaks at enhancer/promoter regions of *PD-L1* and *CD86* in human K562 leukemia cells from ENCODE database (Histone Modifications ChIP-seq from ENCODE/Broad Institute and AP-1 TF ChIP-seq from ENCODE/SYDH) were shown. Red rectangles define the potential enhancers. (B) Jun and Jund binding peaks at enhancer/promoter regions of *PD-L1* and *CD86* in mouse CH12 cells from ENCODE database/SU were shown.

Figure S9. Evaluation of H3K27ac levels at several dysregulated gene loci.

(A) H3K27ac peaks at enhancer/promoter regions of *Fos*, *Jun*, *Jund*, *PD-L1* and *CD86* in mouse from ENCODE database (USCD) were shown. Histone H3K27ac levels at the *Fos*, *Jun*, *Jund*, *PD-L1*, and *CD86* enhancer/promoter regions were analyzed using ChIP-qPCR in BM cells from moribund $Nras^{G12D/+}$; $Asxl1^{-/-}$(NA) mice with AML and age-matched control (C), $Asxl1^{-/-}$ (Asxl1-/-), and $Nras^{G12D/+}$ (Nras) mice. Rabbit IgG was used as a negative control (n=3). (B) mRNA levels of *Fos*, *Jun*, *Jund*, *PD-L1*, and *CD86* were analyzed using RT-qPCR in BM cells from moribund $Nras^{G12D/+}$; $Asxl1^{-/-}$(NA) mice with AML and age-matched control (C), $Asxl1^{-/-}$ (Asxl1-/-), and $Nras^{G12D/+}$ (Nras) mice. Data are presented as mean + SD. Statistical analysis was performed in comparison with those in WT cells. *, $P<0.05$; **, $P<0.01$; ***, $P<0.001$.

Figure S10. Combined inhibition of MEK and BET inhibits *Nras$^{G12D/+}$; Asxl1$^{-/-}$* and *Nras$^{G12D/+}$* CMML cell growth in vitro.

CMML cells from *Nras$^{G12D/+}$; Asxl1$^{-/-}$* (NA) and *Nras$^{G12D/+}$* (Nras) mice were cultured in triplicate in 96-well plates in the presence of DMSO or various concentrations of trametinib and/or GSK525762 for 7 days. Cell numbers were quantified using the CellTiter-Glo assay. Combination Index was calculated using CompuSyn algorithm. The index value less than 1 indicates synergism. Data are presented as mean + SD. * P<0.05; ** P<0.01; *** P<0.001.

Figure S11. Combined inhibition of MEK and BET downregulates inhibitory immune checkpoint pathways in the spleens and livers of *Nras$^{G12D/+}$; Asxl1$^{-/-}$* AML recipient mice.

Sub-lethally irradiated mice were transplanted with $2.5x10^5$ bone marrow cells from moribund primary recipients with *Nras$^{G12D/+}$; Asxl1$^{-/-}$* AML. At 2 weeks after transplantation, mice were randomly separated into two groups, treated with vehicle or combined trametinib and GSK525762 daily for ~3 weeks, and sacrificed for analysis. (A) H&E staining showed the tumor burden (tumor cells in blue line) in BM, spleen, liver and lung. Scale bar, 100μm. (B) Quantification of leukemia cells ($CD45.2^+$) expressing PD-L1/L2, CD155, CD86, or CD80 in SP and liver. (C) Quantification of host derived $CD4^+$ and $CD8^+$ T cells expressing PD-1, TIGIT, or CTLA4 in SP and liver. Data are presented as mean + SD. * P<0.05; ** P<0.01; *** P<0.001.

Figure S12. Combined inhibition of MEK and BET downregulates H3K27ac level in NA-AML cells.

Sub-lethally irradiated mice were transplanted with $2.5x10^5$ bone marrow cells from moribund primary recipients with *Nras*$^{G12D/+}$; *Asxl1*$^{-/-}$ AML. Two weeks after transplantation, mice were randomly separated into two groups, treated with vehicle or combined trametinib and GSK525762 daily for ~3 weeks, and sacrificed for analysis. Expression levels of various histone marks were quantified in leukemia cells ($CD45.2^+$) using flow cytometry. Data are presented as mean + SD. *** P<0.001.

Figure S13. A model of *Nras*$^{G12D/+}$; *Asxl1*$^{-/-}$ CMML/AML.

Asxl1$^{-/-}$ and *Nras*$^{G12D/+}$ synergize to upregulate surface Flt3 expression, hyperactivate ERK signaling, acquire additional recurrent genetic mutations, and aberrantly regulate histone marks to potentially activate gene transcription. These lead to further upregulation of AP1 onco-transcriptome, upregulation of inhibitory immune checkpoint pathways, and T cell exhaustion. Together, these events accelerate NA-CMML progression and promote AML transformation. Upon combined inhibition of MEK and BET, AP1 onco-transcriptome and inhibitory immune checkpoint pathways are downregulated, T cell exhaustion phenotype is partially rescued, cytotoxicity of CD8 T cells is enhanced, and NA-AML progression is slowed down.

Figure S1-Zhang

A

		MSC 2	A2HSC	A3HSC	LTHSC	STHSC	CMP	GMP	T-cell	CD33+	CD45+
Moffitt-1	TET2	0		0.22	0.14	0.27	0.23	0.20	0.11	0.23	0.24
	KRAS	0		0.20	0.44	0.01	0.39	0.34	0	0.41	0.42
	ASXL1	0.01		0.43	0.20	0.75	0.50	0.41	0.24	0.47	0.43
Moffitt-2	NRAS	0	0.14	0.41			0.14	0.98	0	0.45	0.45
Moffitt-3	TET2			0.06			0.09	0.94	0.01	0.50	0.22
	KRAS			0			0	0	0	0.44	0.19

B

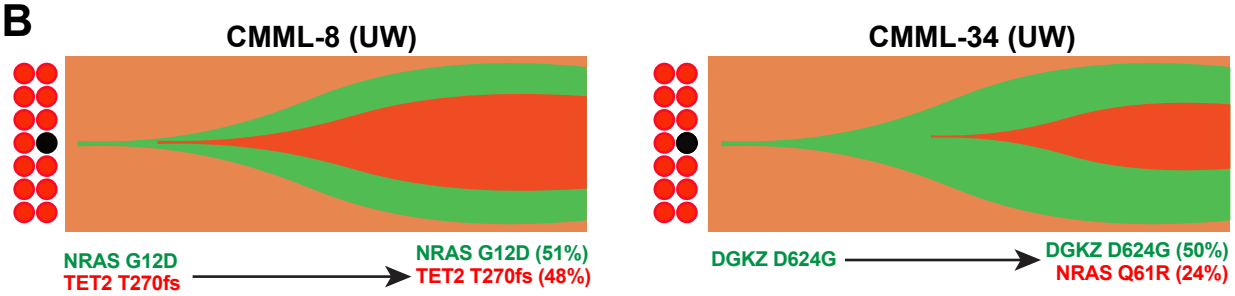

Figure S2-Zhang

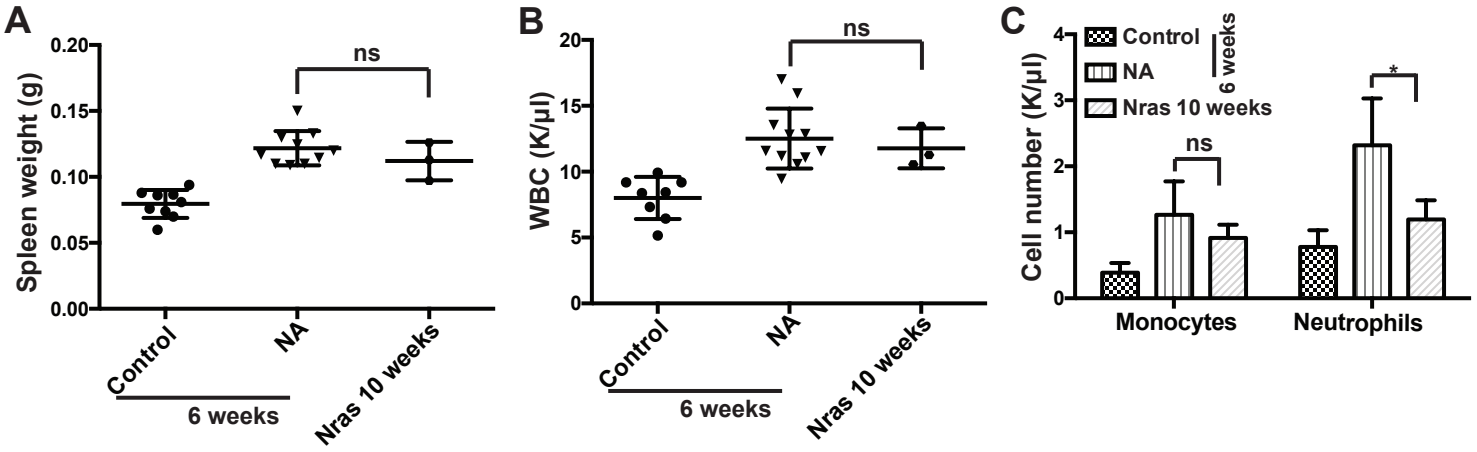

A

Recurrent mutations in >=3/4 mice		NA-CMML# 1	2	3	4	CMML patient samples n=174 Gustave Roussy Cancer Center and Mayo clinic
ATP-binding	Abca13					0
	Abca2					0
Protein Kinase	Ttn					4
	Phactr4					0
Epigenetic regulation	Kdm4a					0
	Ncapg2					0
	Cfap46					0
	Kdm5a					0
	Dnah7a					0
G protein pathway	Sbf2					1
	Celsr3					1
	Obscn					0
	Trio					0
	Kctd8					0
Ubiquitin pathway	Hectd4					0
	Ubr4					0
	Lrp1b					1
KICSTOR Complex	Szt2					2
	Dst					2
Transmembrance transporter	Trdn					1
	Pkd1l2					0
Notch pathway	Notch1					0
Tumor suppressor	Dlec1					0
Structural proteins	Speg					0
	Myom2					1
	Myo9a					0
	Dnah8					2
	Fbn2					1
	Myh15					0
	Amer1					1
	Lrp1					0
	Boc					1
Others	Myo5b					0
	Hmgxb3					0
	Ift140					0
	Mmrn1					0
	Lmo7					0
	Zbtb40					0
	Spag17					0
	Oas3					0
	Cog7					0

B

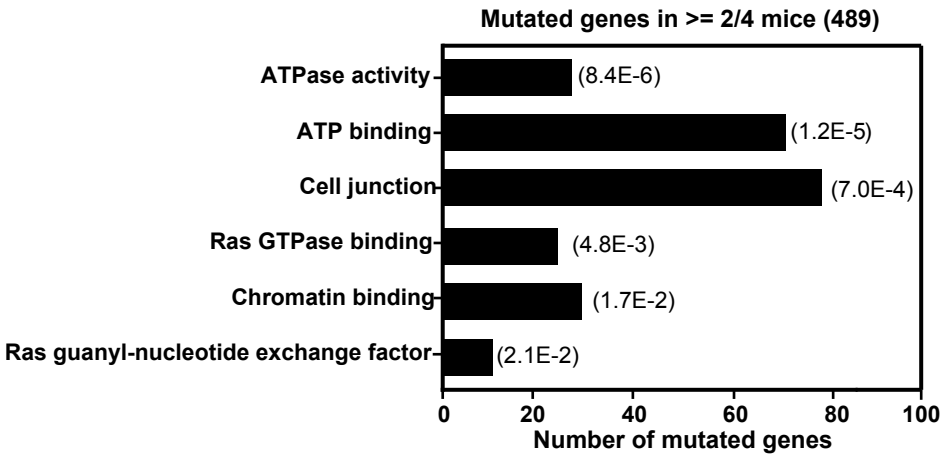

Figure S4-Zhang

A

Recurrent mutations in >=4/6 mice		NA-AML#						AML Patient Database			Transformed AML
		1	2	3	4	5	6	OHSU n=562	TCGA n=200	WashU n=116	Mayo n=36
Transcription	Bicra							0	0	0	0
	Trrap							4	1	0	0
Tumor suppressor	Csmd2							9	1	0	0
	Ptprf							1	1	0	0
	Herc1							2	3	1	1
Protein Kinase	Phactr4							2	1	0	0
	Ttn							0	16	1	0
Cell signaling	Phldb1							2	0	0	0
	Ascc3							1	0	0	1
Structural proteins	Diaph3							0	0	0	1
	Plec							0	1	0	0
Others	Kdf1							1	0	0	0

Missense 0 0.2 0.4 0.6 0.8

Frameshift 0 0.2 0.4 0.6 0.8

B

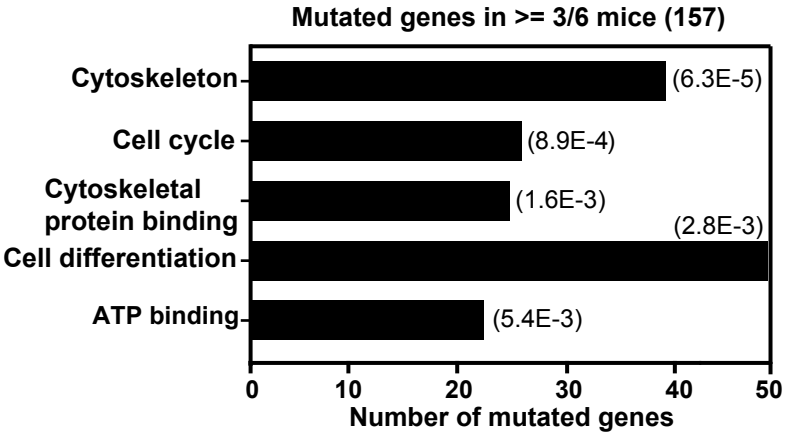

C

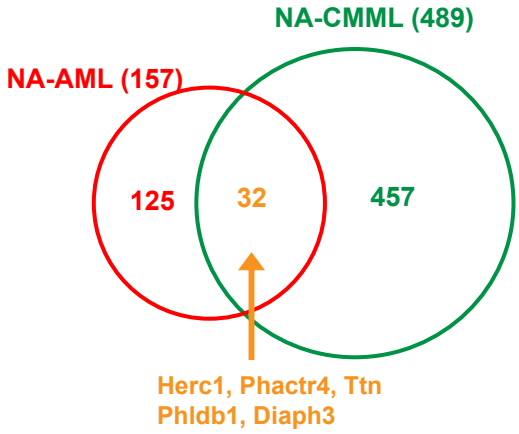

Figure S5-Zhang

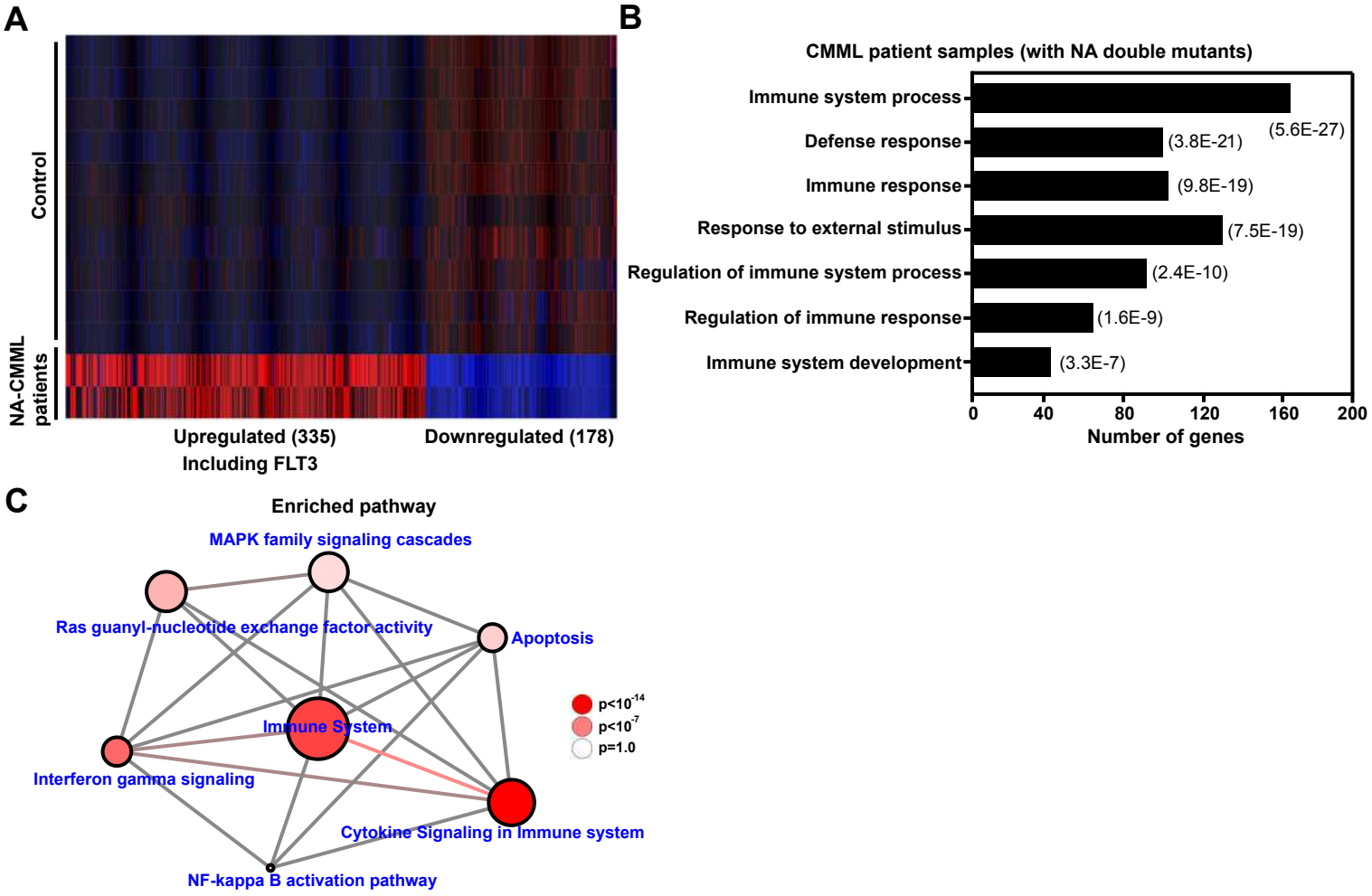

Figure S6-Zhang

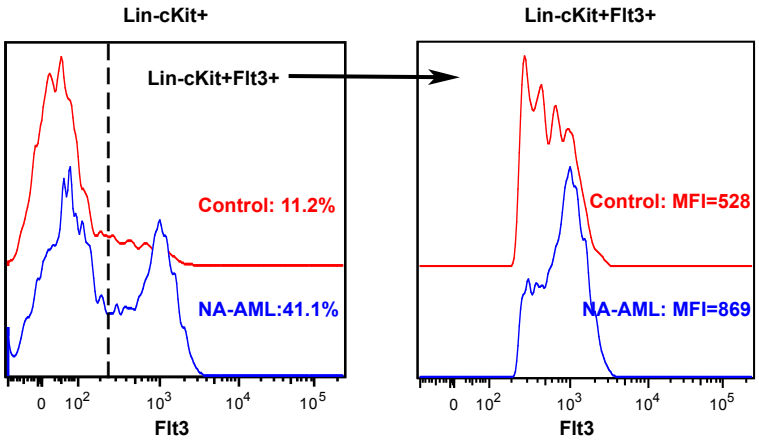

Figure S7-Zhang

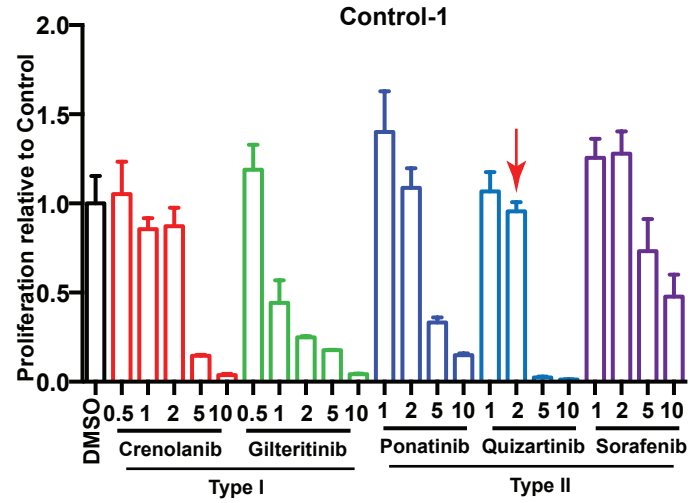

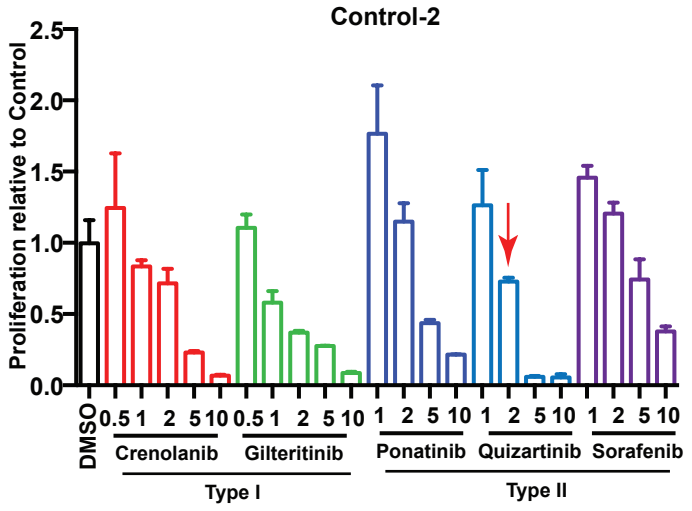

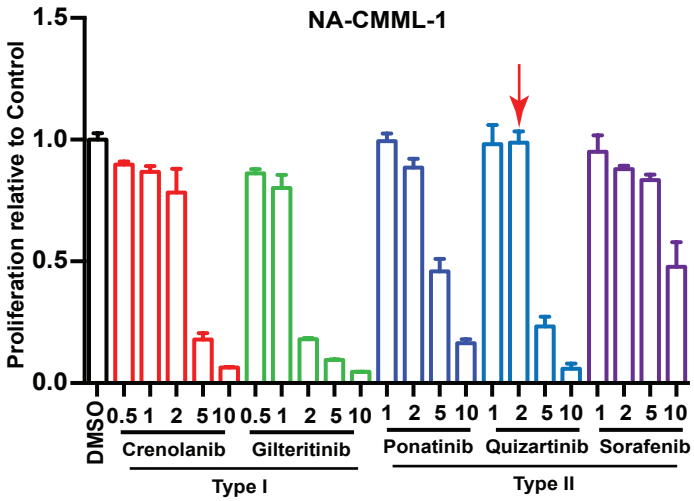

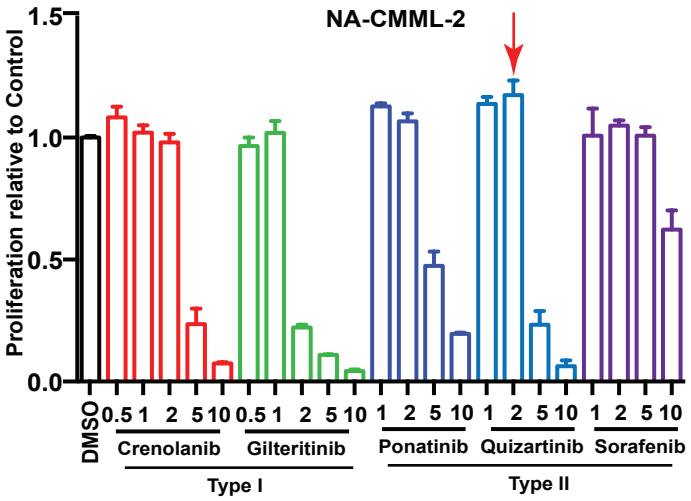

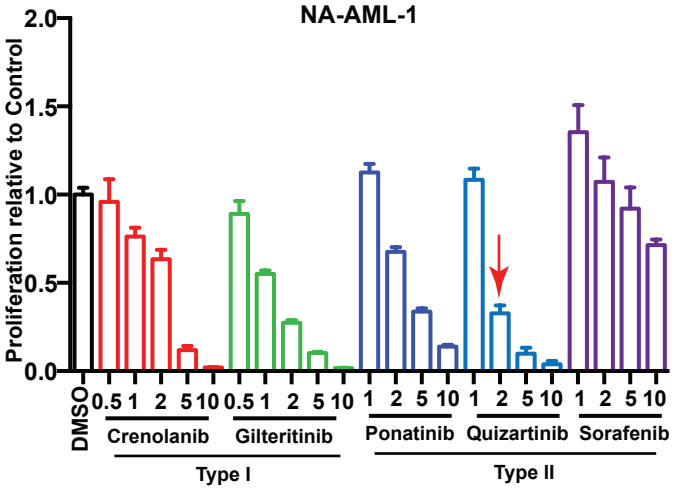

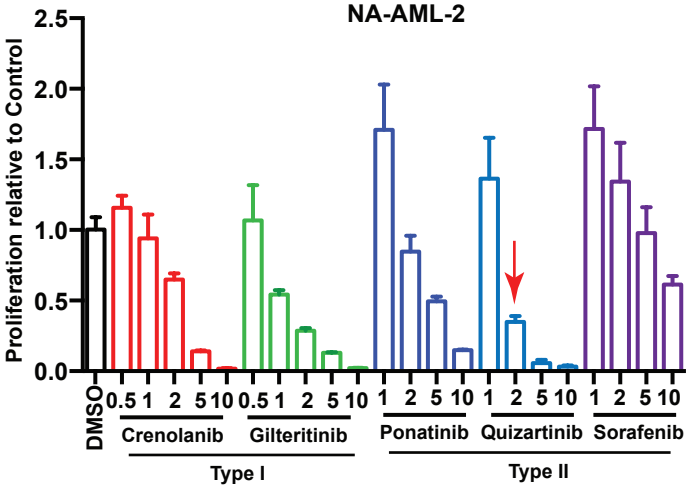

Figure S8-Zhang

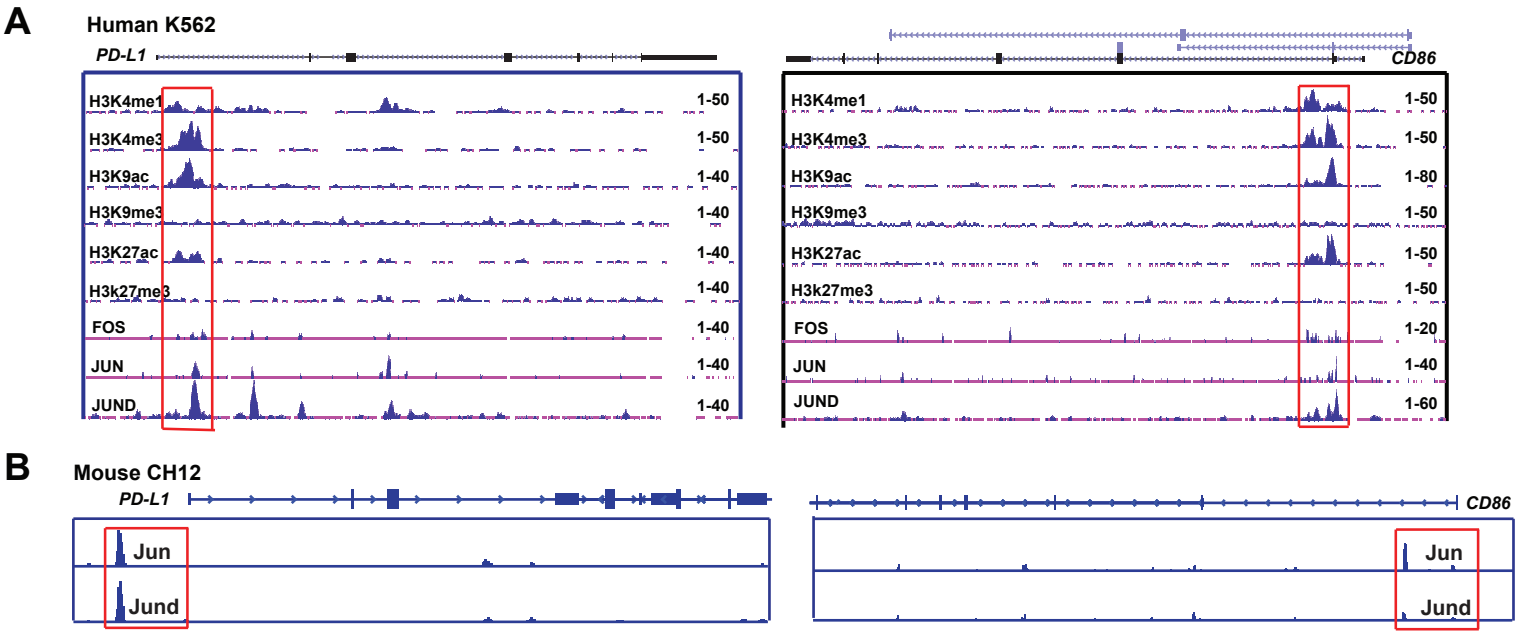

Figure S9-Zhang

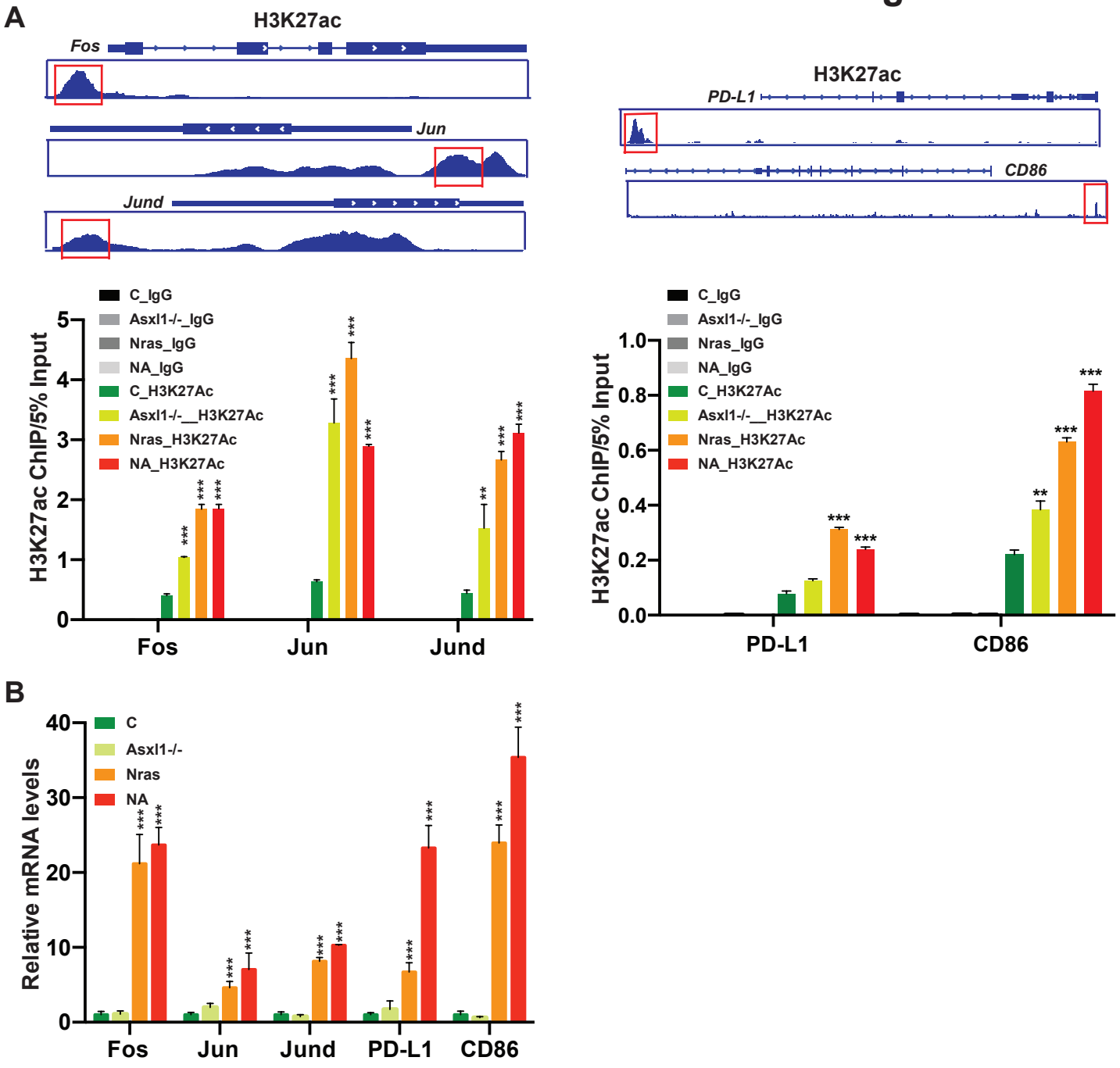

Figure S10-Zhang

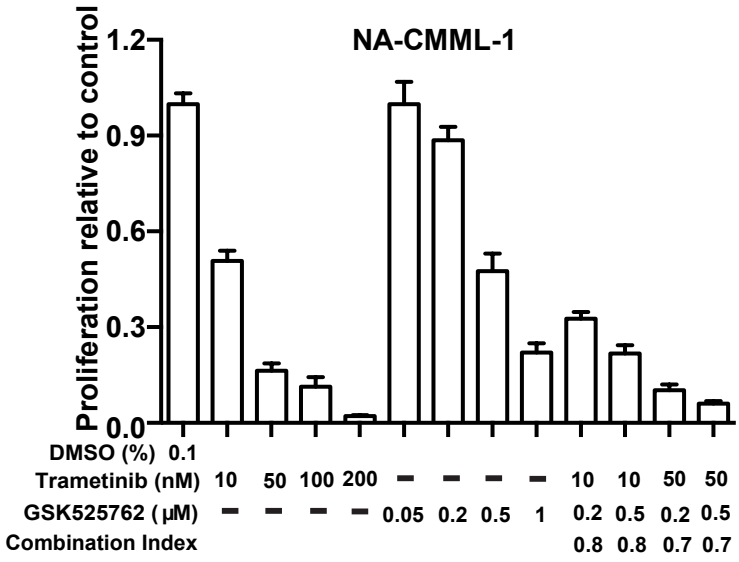

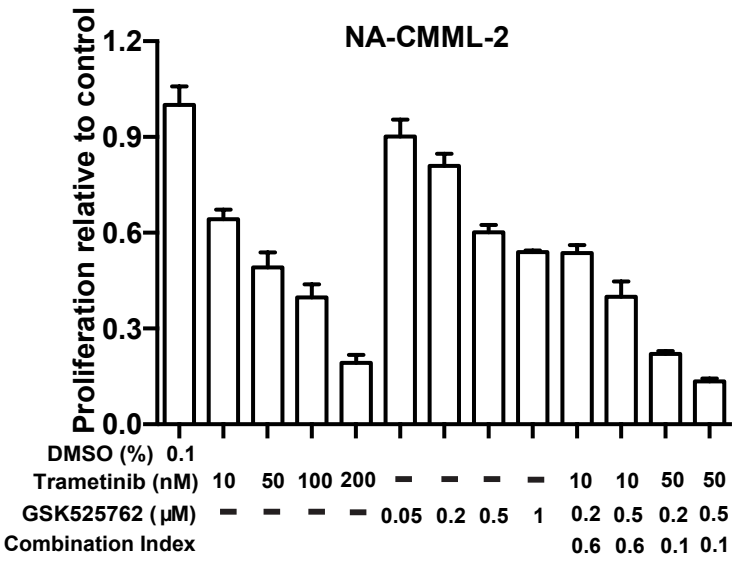

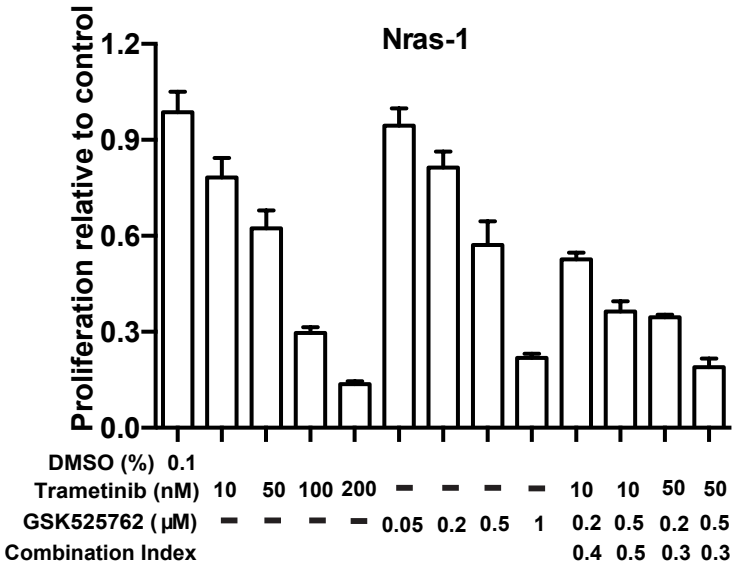

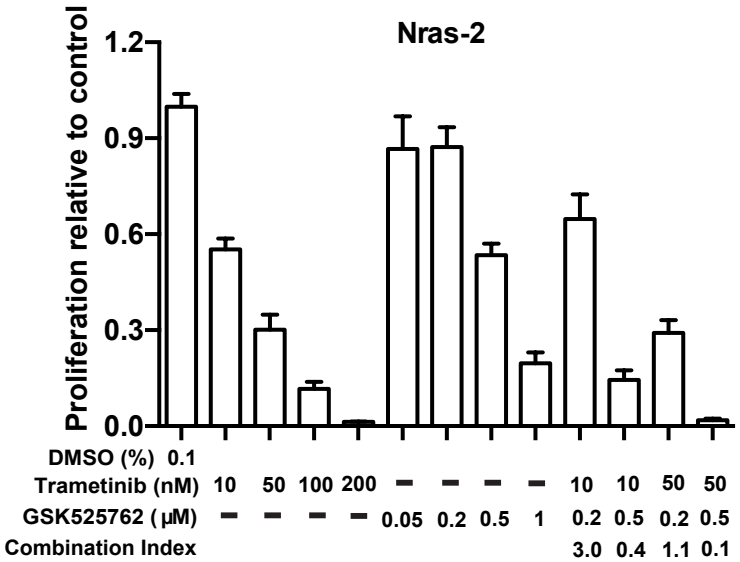

Figure S11-Zhang

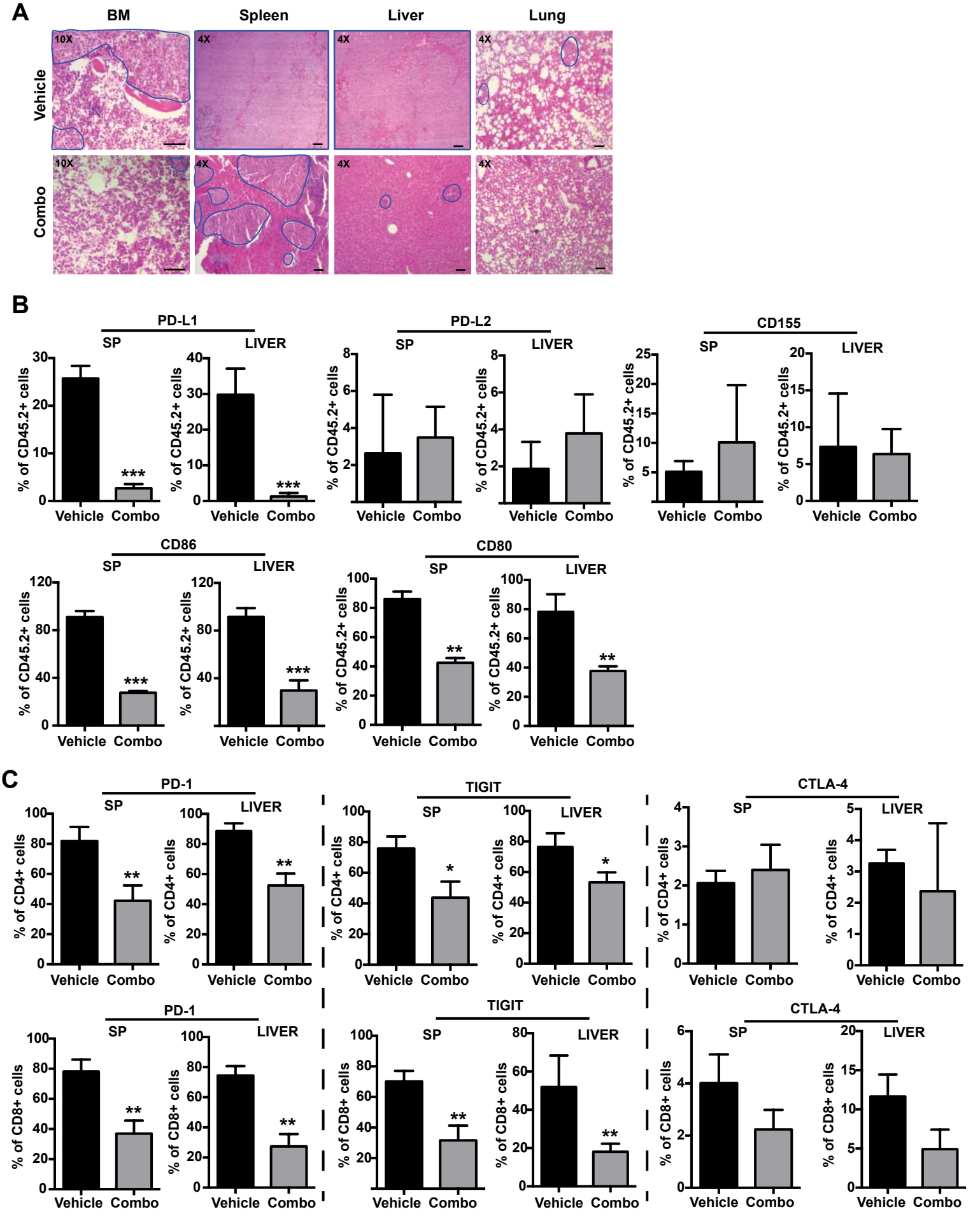

Figure S12-Zhang

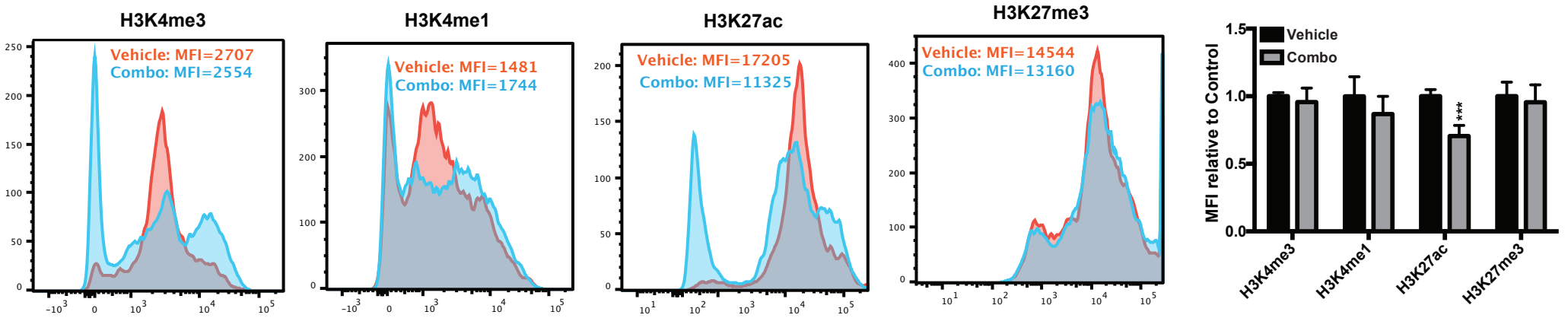

Table S1. Summary of NRAS and ASXL1 mutations in myeloid and T cells from NA-CMML patients

Case #	CD14+ monocytes		CD3+ T cells	
	NRAS (VAF)	ASXL1 (VAF)	NRAS (VAF)	ASXL1 (VAF)
Mayo-1	G12D (43%)	R1068X (36%)	0%	0%
UPN18	G12A (49%)	Q760X (56%)	0%	Q760X (0.6%)
UPN46	G12S (27%) G13V (20.6%)	G643fs (40.2%)	G12S (3%) G13V (0.8%)	G643fs (5.8%)
UPN49	G13V (45%)	G643fs (36%)	G13V (5.1%)	G643fs (1.6%)
2186	G12V (47.7%)	G642fs (43.3%)	G12V (4.4%)	G642fs (2.9%)
2202	G12V (12.7%)	G629fs (32.6%)	G12V (3.4%)	G629fs (1.7%)
2264	G12D (44.7%)	G642fs (28.3%)	G12D (8.4%)	G642fs (3.4%)
2238	Y64D (46%)	G642fs (5.8%)	Y64D (4.8%)	G642fs (0.4%)

Note: CD14+ monocytes and CD3+ T cells were purified/enriched using magnetic beads as described in the Supplemental Materials and Methods. The enriched T cells may have various degrees of contamination from myeloid cells.

Figure S13-Zhang